Forcing of the Atlantic Equatorial Deep Jets Derived from Observations

Martin Claus, Richard J. Greatbatch, and Peter Brandt

GEOMAR Helmholtz Centre for Ocean Research Kiel, Kiel, Germany

John M. Toole

Woods Hole Oceanographic Institution, Woods Hole, Massachusetts

ABSTRACT

The equatorial deep jets (EDJs) are a ubiquitous feature of the equatorial oceans; in the Atlantic Ocean, they are the dominant mode of interannual variability of the zonal flow at intermediate depth. On the basis of more than 10 years of moored observations of zonal velocity at 23°W, the vertically propagating EDJs are best described as superimposed oscillations of the 13th to the 23rd baroclinic modes with a dominant oscillation period for all modes of 1650 days. This period is close to the resonance period of the respective gravest equatorial basin mode for the dominant vertical modes 16 and 17. It is argued that since the equatorial basin mode is composed of linear equatorial waves, a linear reduced-gravity model can be employed for each baroclinic mode, driven by spatially homogeneous zonal forcing oscillating with the EDJ period. The fit of the model solutions to observations at 23°W yields a basinwide reconstruction of the EDJs and the associated vertical structure of their forcing. From the resulting vertical profile of mean power input and vertical energy flux on the equator, it follows that the EDJs are locally maintained over a considerable depth range, from 500 to 2500 m, with the maximum power input and vertical energy flux at 1300 m. The strong dissipation closely ties the apparent vertical propagation of energy to the vertical distribution of power input and, together with the EDJs' prevailing downward phase propagation, requires the phase of the forcing of the EDJs to propagate downward.

1. Introduction

The equatorial deep jets (EDJs) are vertically alternating, stacked zonal jets along the equator that are a feature of all equatorial ocean basins. They were first discovered in the Indian Ocean by Luyten and Swallow (1976) and subsequently observed in the Pacific (Hayes and Milburn 1980; Leetmaa and Spain 1981; Firing 1987; Johnson et al. 2002) and Atlantic Oceans (Eriksen 1982; Gouriou et al. 2001; Johnson and Zhang 2003; Bunge et al. 2008; Brandt et al. 2011). In the Atlantic, the EDJs are the dominant signal of interannual zonal velocity variability at the intermediate depth range spanning

from 200 to 3000 m (Brandt et al. 2011). They have amplitudes of up to 20 cm s^{-1} with vertical scales ranging from 300 to 700 m and zonal scales comparable to the width of the basin (Bourlès et al. 2003; Johnson and Zhang 2003; Bunge et al. 2008; Brandt et al. 2011). Moored current meter observations at 10° (Bunge et al. 2008) and 23°W (Bunge et al. 2008; Brandt et al. 2011) revealed an unambiguous downward phase propagation of the EDJs with an associated time scale of about 4.5 yr. This is consistent with phase estimates by Johnson and Zhang (2003) based on a large body of hydrographic station data and these authors, among others, noted the good correspondence of the EDJs to linear first meridional mode Rossby wave dynamics. Notably, the meridional structure of the EDJs is 50% wider than what is expected based on linear theory, given their observed vertical scale (Johnson and Zhang 2003; Youngs and Johnson 2015).

In the presence of a mean zonal tracer gradient and dissipation, linear waves are able to produce a time-mean tracer flux down the gradient. Indeed, Gouriou et al. (2001)

Corresponding author address: Martin Claus, GEOMAR Helmholtz Centre for Ocean Research Kiel, Düsternbrooker Weg 20, 24105 Kiel, Germany.
E-mail: mclaus@geomar.de

found evidence that the EDJs transport CFC-11 rich North Atlantic Deep Water along the equator from within the deep western boundary current (DWBC) to at least 35°W. Based on an advection–diffusion model driven by an EDJ-like flow field, Brandt et al. (2012) found a good correspondence between the modeled and observed oxygen variability at the equator and inferred a net eastward flux of oxygen along the equator. These results point to the importance of the EDJs, but also of the mean equatorial intermediate current system (EICS), as defined by Ascani et al. (2010), for determining the mean distribution of tracers and their variability in the equatorial Atlantic Ocean. However, these current systems are not well represented or missing in state-of-the-art ocean general circulation models (OGCMs; Ascani et al. 2010, 2015). Dietze and Loeptien (2013) argue that the persisting problem of too little oxygen in the deep eastern equatorial basins in Earth system models can be attributed to this model deficiency, and Getzlaff and Dietze (2013) supported this argument by parameterizing the effect of the EICS and EDJs as an enhanced zonal diffusivity, which led to improved distributions of temperature, salinity, oxygen, and nutrients in their model.

The simplest model of the EDJs is an equatorial basin mode (Cane and Moore 1981), which is an eigenmode of a zonally bounded equatorial basin. It consists of an equatorial Kelvin wave and the gravest equatorial long Rossby wave, which reflect at the eastern and western boundary, respectively. The characteristic period of the basin mode is the sum of the time it takes each wave to cross the basin. The observed scales of the EDJs show good correspondence to the characteristics of the gravest equatorial basin mode of the dominant vertical normal mode in each equatorial basin (Youngs and Johnson 2015). Also, features in idealized numerical models resembling the EDJs show a similar correspondence (D'Orgeville et al. 2007). Furthermore, Ascani et al. (2015) and Matthießen et al. (2015) reported close correspondence of the EDJs in their nonlinear model to the analytical solution of a dissipative linear equatorial basin mode.

In the framework of linear wave dynamics, the observed downward phase propagation of the EDJs implies upward energy propagation (Gill 1982), which requires a source of energy at depth and a sink near the ocean surface. Indeed, Brandt et al. (2011) found evidence of observed surface climate variability in the equatorial Atlantic region at the period of the Atlantic EDJs and argued that this variability is driven by the surface expression of the EDJs. Also Matthießen et al. (2015) found a linkage in time scale between the variability of the North Equatorial Countercurrent (NECC)

and the EDJs in their model and argued, based on the diagnosed vertical energy flux, which was shown to be upward, that this is an impact of the EDJs on the NECC. However, the source of energy feeding the EDJs still remains unclear. A promising candidate is the rectification of deep, equatorial, intraseasonal variability in the form of short Yanai waves to generate or maintain the EDJs. There are two proposed mechanisms. First, Hua et al. (2008) demonstrated that zonally short Yanai waves of large vertical scale and westward phase propagation, which are subject to barotropic shear instability, destabilize and form stacked equatorial zonal jets of small vertical scale. The vertical scale of these jets is set by the zonal scale of the basic Yanai wave, a finding that was confirmed by idealized numerical simulations (D'Orgeville et al. 2007; Ménesguen et al. 2009) and is consistent with a more realistic model configuration (Eden and Dengler 2008), in which Yanai waves are shed by fluctuations of the DWBC. However, these simulations have difficulty capturing the direction of vertical propagation. Second, Ascani et al. (2015) showed that in idealized numerical simulations, pairs of short intraseasonal Yanai waves produced by the unstable equatorial surface currents interact nonlinearly via the meridional advection term (vu_y) in the zonal momentum equation and drive vertically stacked equatorial jets that resemble the observed Atlantic EDJs. Although this mechanism can explain the maintenance of EDJs, it cannot account for the selection of their vertical scale and the direction of vertical propagation. It should be noted here that the internal wave field might also maintain the EDJs in the context of wave–mean flow interactions by momentum flux divergence, which acts to sustain the vertical shear between individual jets (Muench and Kunze 1999, 2000).

Although the EDJs are often modeled as linear equatorial basin modes, the jets themselves are not fully linear. Ascani et al. (2015) showed that in their numerical representation of the EDJs, the nonlinear interaction of the EDJs, via the zonal advection term (uu_x) in the zonal momentum equation, is one of the major sinks of energy for the EDJs in their model, transferring energy to the time-mean, large vertical scale Lower Equatorial Intermediate Current (Firing et al. 1998). Additionally, as noted above, the vu_y terms are thought to act predominantly as forcing terms for the EDJs via the nonlinear interaction of intraseasonal Yanai waves (Ascani et al. 2015), which are independent of the EDJs. It follows that the nonlinear terms in the zonal momentum budget can be parameterized as a dissipation and forcing in a linear model of the EDJs.

Regardless of the actual driving mechanism, the EDJs must be maintained over a considerable depth range

while they propagate vertically. This becomes apparent from an estimate of the effective lateral diffusivity that is felt by the EDJs and acts to broaden their meridional structure with respect to inviscid linear theory. To obtain the observed 50% broadening that is observed in the Atlantic (Johnson and Zhang 2003), Greatbatch et al. (2012) estimated a required effective diffusivity A_{eff} of 100 to $300 \, \text{m}^2 \, \text{s}^{-1}$. This estimate does not change substantially if the effect of the barotropic mean flow on the wave field is considered (Claus et al. 2014). Interestingly, a broadening of similar magnitude is also observed in the Pacific and Indian Oceans (Muench et al. 1994; Youngs and Johnson 2015). With a given meridional scale L_θ of roughly 120 km (Youngs and Johnson 2015), the corresponding dissipation time scale T_ν for the Atlantic EDJs, given by

$$T_\nu = \frac{L_\theta^2}{A_{\text{eff}}}, \tag{1}$$

ranges from 1.5 to 4.7 yr, which is about the same or less than the oscillation period of the EDJs. Hence, in the absence of forcing, an individual jet would have difficulty propagating vertically a distance greater than its vertical scale. In the presence of such strong damping, it can be conjectured that the apparent vertical propagation of energy is closely tied to the vertical distribution of power input into the EDJ current system. Moreover, because of strong dissipation, it is also unlikely that the EDJs feel the influence of the bottom topography if the forcing is confined to a depth range well above the shallowest bathymetric feature of the open equatorial Atlantic, that being the Mid-Atlantic Ridge.

As noted above, several driving mechanisms have been proposed in the literature so far (e.g., Muench and Kunze 1999; Hua et al. 2008; Ascani et al. 2015), based on either theoretical considerations or idealized numerical modeling. To better understand the relative importance of these mechanisms in the real ocean, an observational estimate of the required momentum input into the EDJs would be useful. Therefore, we address the following question: What forcing is required to obtain vertically propagating linear waves that have the same properties as the observed EDJs in the Atlantic Ocean? Our analysis is based on moored, long-term, near-full-depth observations of zonal velocity on the equator at 23°W. These observations are used to extract the EDJ signal expressed in terms of vertical normal modes. Furthermore, the linearity of the phenomenon, expressed by the close correspondence of the EDJs to the gravest linear equatorial basin mode, is exploited to obtain amplitude and phase information for each vertical normal mode by means of a linear shallow-water

model. On this basis, the required magnitude and vertical structure of the forcing can be estimated and the Atlantic EDJ signal can be reconstructed throughout the basin, facilitating quantification of both the power input and vertical energy flux.

The structure of this paper is as follows: Section 2 describes the fit of zonal velocity observations on the equator at 23°W to a set of vertically propagating waves. This shows that most of the variability of the zonal flow projects on three frequencies, corresponding to the semiannual, annual, and 1650-day period, of which the longest is associated with the EDJs. In section 3, the response of a shallow-water model for each vertical normal mode (hereafter denoted as the multimode model) is obtained, in which each mode is driven by a harmonic forcing that oscillates at the frequency of the EDJs, as diagnosed in section 2. A summed multimode model solution is subsequently derived by scaling and phase shifting each mode so that it matches the fitted observations on the equator at 23°W. The resulting set of scaling coefficients and respective phases describe the vertical time structure of the forcing required to drive the Atlantic EDJs in a linear system. The scaled multimode solution gives a reconstruction of the EDJs' signal throughout the equatorial Atlantic basin and an analysis of the associated power input and vertical flux of energy is provided. In section 4, the results are summarized and discussed.

2. Observational analysis

In what follows, it will be described how the observations of zonal velocity on the equator at 23°W were obtained and what data were used to estimate the mean stratification of the tropical Atlantic basin, an important parameter for determining the vertical structure functions of the baroclinic modes and the associated gravity wave speeds required to configure the multimode model in section 3. Furthermore, a linear decomposition of the zonal velocity observations into vertically propagating waves, expressed in terms of vertical normal modes, is described. This decomposition reveals that the variability of the zonal flow has three dominant periods (semiannual, annual, and 1650 days) and that for each of these periods, the energy is mostly contained in the vertical mode that forms a resonant equatorial basin mode close to that period. The analysis further elucidates the vertical structure of EDJs.

a. Mean stratification and zonal velocity data

An essential part of our approach involves the fitting of the observed zonal velocity on the equator at 23°W to vertical normal modes. Consequently, an accurate

TABLE 1. Cruises during which the profiles were taken that were used to compute the mean stratification at 23°W on the equator.

Cruise	Date
Meteor 68/2	June 2006
Meteor 80/1	November 2009
Maria S. Merian 18/2	May 2011
Maria S. Merian 22	November 2012
Meteor 106	May 2014

representation of the mean stratification at the location of the observations is required. In the present work, conservative temperature, pressure, and salinity profiles from 47 CTD casts are used. These casts were collected within 50 km of the equator near 23°W during five cruises (listed in Table 1). Only those profiles that reach down to at least 1200 m were used. The individual temperature and salinity profiles were bin averaged on a uniform 10-m vertical grid to a maximum depth of 4500 m. Then, for each cast separately, the buoyancy frequency profile was computed from the locally referenced potential density, and these profiles were averaged to obtain the mean stratification used to deduce the structure functions and gravity wave speeds associated with the corresponding vertical normal modes. Brandt et al. (2008) showed that most of the Atlantic EDJ signal is contained in a broad band spanning baroclinic modes 7 to 25, which is why in this work the first 40 normal modes are used in order to resolve the observed vertical scales. The vertical structure functions of pressure $\hat{p}_n$ were normalized, so that they form an orthonormal set.

For the objective of the present work, a dense, deep-reaching, and long set of observations are of invaluable importance. Hence, we use processed zonal current measurements from the subsurface mooring at 23°W on the equator, collected from February 2004 to May 2014 (Fig. 1). The upper part of the water column was covered

by two acoustic Doppler current profilers (ADCPs) sampling a depth range from near the surface to 600–800 m and provided, after detiding and subsampling, velocity data with daily resolution (Brandt et al. 2012). The depth range between 1000 to 3500 m was covered by a McLane Moored Profiler (MMP) from which the data could be successfully recovered at least in parts for three deployment periods of about 1.5 yr each. These instruments measure various state parameters, including zonal velocity, while moving along the mooring cable, which takes about 3 h for one profile. The upward and downward profiles were separated by 6 h with these paired profiles acquired every 4 days. The gap between the ADCP and MMP measurements was bridged by single-point current meters at varying depths, depending on the deployment period. All data from the three different sets of devices were mapped on a common grid having a temporal resolution of 7 days and the same vertical axis as the normal-mode dataset. The deepest valid values of zonal velocity were used to extend the dataset down to 4500 m, but only if the measurement was taken below 3000 m.

b. Harmonic normal-mode decomposition of zonal velocity

The observed zonal velocity is fit in a least squares sense to a set of steadily oscillating, vertically propagating linear waves, each of them expressed as a sum of vertical normal modes based on the assumption of a flat bottom (Gill 1982). Let Ω be the set of angular frequencies of the considered waves and N the number of vertical normal modes taken into account, then

$$u(z,t) = \sum_{\omega \in \Omega} \sum_{n=1}^{N} [(a_{n\omega}e^{i\omega t} + a_{n\omega}^* e^{-i\omega t}) + a_{n0}]\hat{p}_n(z) \qquad (2)$$

denotes the linear fitting model, where z is the vertical coordinate, t is the time, $a_{n\omega}$ and $a_{n\omega}^*$ are the
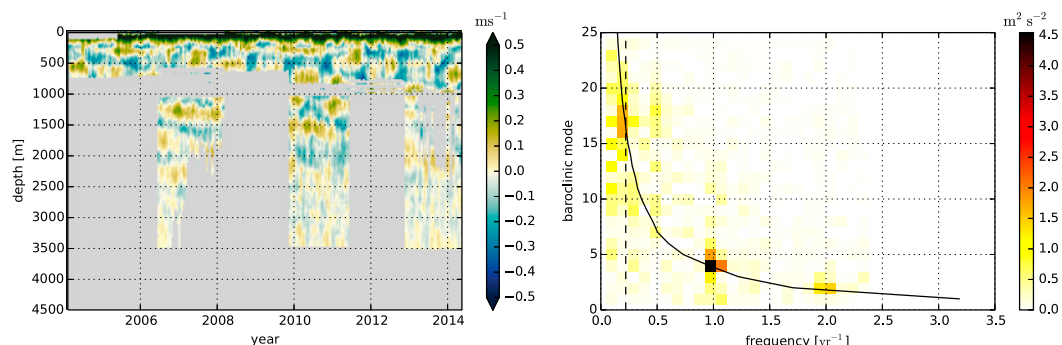

FIG. 1. (left) Moored zonal velocity observations at 23°W on the equator. (right) Fitted energy spectrum of the zonal velocity data shown on the left panel for each baroclinic mode. See text for a detailed description of the fitting procedure. The solid line marks the resonance frequency of the gravest equatorial basin mode and the dashed line corresponds to a period of 1650 days, which explains most variability in the interannual range.

complex-valued fitting coefficients for the set of waves, and a_{n0} is the real-valued coefficient for the mean flow structure. The $\hat{p}_n$ is the vertical structure function for pressure of the nth vertical normal mode, which is obtained from the estimate of the mean stratification described in the previous subsection. Although the asterisk denotes the complex conjugate, the fitting routine is not constrained to abide by this identity but rather treats $a_{n\omega}$ and $a_{n\omega}^*$ as independent parameters, and a check for consistency is applied after the fitting is done. Similarly, a_{n0} is not constrained to be real valued but is treated as complex valued. To arrive at an estimate of the linear signal associated with the EDJs, a set of the dominant frequencies and the time–mean flow are simultaneously fit to the observed data to reduce the effect of aliasing, which would be more pronounced if single frequencies were fit independently.

c. Results

To arrive at a credible estimate of the EDJ structure based on observations, the dominant modes of linear variability and the associated periods must be identified. Therefore, (2) was repeatedly fit to the zonal velocity data for a single but varying frequency corresponding to periods ranging from 14 to 3752 days. The sampled frequencies are the same as would result from a discrete Fourier transform of a complete time series with the same length ($\sim$10 yr) and sampling frequency (7 days) as the data used here. Although the modal energy estimate following this approach, shown in Fig. 1, might be subject to aliasing, it still gives a good indication of which periods are important. Most of the total variability appears to be captured by three distinct frequencies: the semiannual cycle, the annual cycle, and a frequency of about 0.2 cycles per year; the latter being the signature of the EDJs. These frequencies together contain about 30% of the estimated total kinetic energy of the zonal flow variability and have peak energy at vertical mode numbers 2, 4, and 17, respectively. Interestingly, all prominent peaks in the modal spectrum are located on the resonance line of the gravest equatorial basin mode, given by

$$\nu_{\mathrm{res}} = \frac{c_n}{4L}, \tag{3}$$

where L is the width of the basin at the equator, here 55° for the Atlantic Ocean, and c_n is the gravity wave speed of the nth vertical normal mode (Cane and Moore 1981). This provides reassurance that our application of linear dynamics in section 3 is appropriate.

While the annual and semiannual cycle are thought to be externally driven by variations of the wind stress due to the seasonal migration of the intertropical convergence
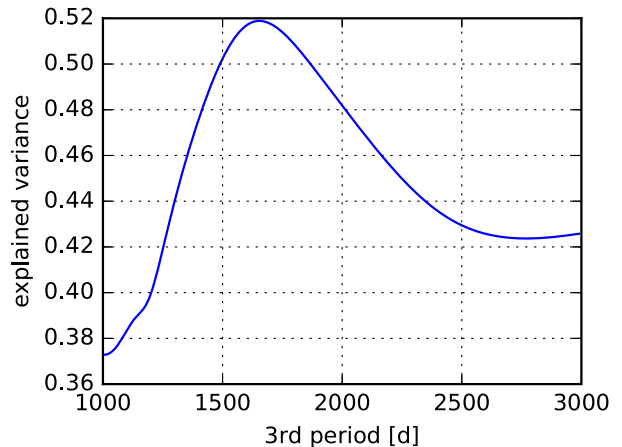
FIG. 2. Fraction of variance of the observed zonal velocity explained by a fit using (2) consisting of three periods: the semiannual cycle, annual cycle, and a period varying between 1000 and 3000 days.

zone (Johns et al. 2014), the frequency of the peak in interannual variability cannot be specified a priori. Hence, a second, repetitive fitting procedure is performed, but now (2) consists of a set of three periods, only with two being fixed as the semiannual and annual cycle and the third period ranging from 1000 to 3000 days at a 10-day increment. Most variance is explained for periods ranging from 1500 to 1800 days with a maximum at 1650 days (Fig. 2). This maximum is close to the 1670-day period found by Brandt et al. (2011), based on a 1.5-yr-long subset of the data used here and is within the error bars of an estimate by Youngs and Johnson (2015), based on CTD profiles from Argo floats and historical shipboard CTD.

The fitted signals resemble, to a very high degree, not only the seasonal variability, for example, of the Equatorial Undercurrent (EUC; Brandt et al. 2016), but also the vertically propagating EDJs. The combined fitted variability of all three periods (semiannual, annual, and 1650 days) explains 52% of the total variance of the observed zonal flow, whereby the 1650-day signal individually explains a similar amount of variability (18%) compared to the annual (27%) and substantially more than the semiannual signal (6%). This high level of explained variance can readily be seen when comparing the original data to the fitted zonal flow, shown in Figs. 3a and 3b, respectively, and demonstrates the importance of the three oscillation periods for explaining the variability of the zonal flow on the equator at 23°W throughout the water column. To verify that the extension of the observed data to the full depth of 4500 m has no substantial impact on the estimated baroclinic structure of the EDJs, the estimated vertical structures
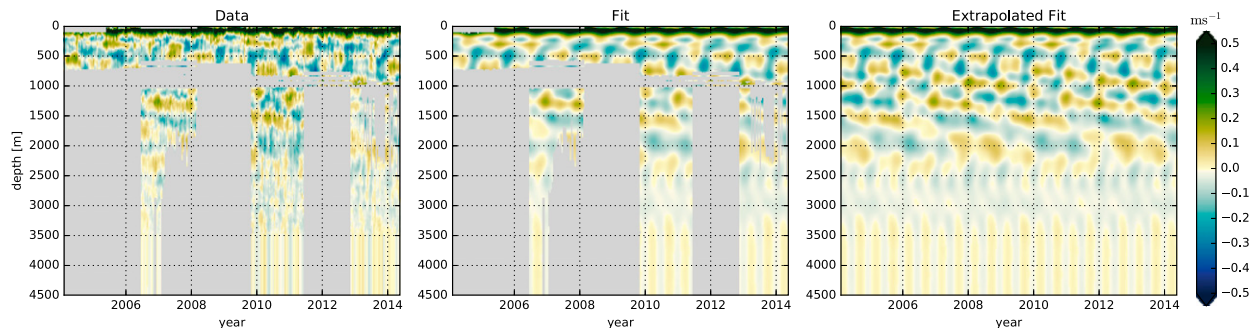
FIG. 3. (a) Zonal velocity at 23°W on the equator with the data extended to full depth as described in the text. (b) Zonal velocity obtained by fitting semiannual, annual, and 1650 days variability and a mean flow to the data shown in the left panel. (c) As in (b), but with the gaps in the data being filled.

were used to extrapolate the fitted signal to fill the gaps in the data. Figure 3c shows that below 3000 m, most of the variability that is not directly constrained by in situ observations is projecting onto the semiannual period.

The baroclinic structure of the fitted EDJ signal in terms of projected zonal velocity amplitude given by $2|a_{n\omega}|$ and the corresponding phase is shown in Fig. 4. The semiannual and annual variability have sharp peaks at the second and fourth baroclinic mode, respectively (Brandt et al. 2016), whereas the 1650-day period has a broad peak ranging from mode 6 to 26. The mode spectrum for the EDJ period is remarkably similar to the baroclinic spectrum estimated by Brandt et al. (2008) from a much shorter subset of the data used here, indicating the robustness of the mode spectrum. The corresponding phase increases with increasing mode number for modes 13 and higher, a necessary requirement for a downward phase propagation. The prevailing downward phase propagation can also be seen in time–depth space above 2500-m depths in the upper-left panel of Fig. 5.

3. Inferring the forcing and basinwide reconstruction of the EDJs

This section starts with the configuration of the multimode model used to determine the linear response of the equatorial Atlantic to zonal forcing that oscillates at the frequency of the EDJs. A method will be described, whereby the response of the multimode model together with the observed vertical structure of the EDJs, estimated in section 2c, can be used to obtain the vertical time structure of the forcing required to drive the Atlantic EDJs in a linear system and to reconstruct the EDJ's signal throughout the equatorial Atlantic basin. Based on this reconstruction, an analysis of the implied power input and vertical energy flux of the EDJs is obtained.

a. Model details

The shallow-water model used for each vertical normal mode has a meridional extent of 20° either side of the equator, and the coastline follows the 1000-m isobath of the equatorial Atlantic basin. The equivalent depth for each mode is chosen so that the associated
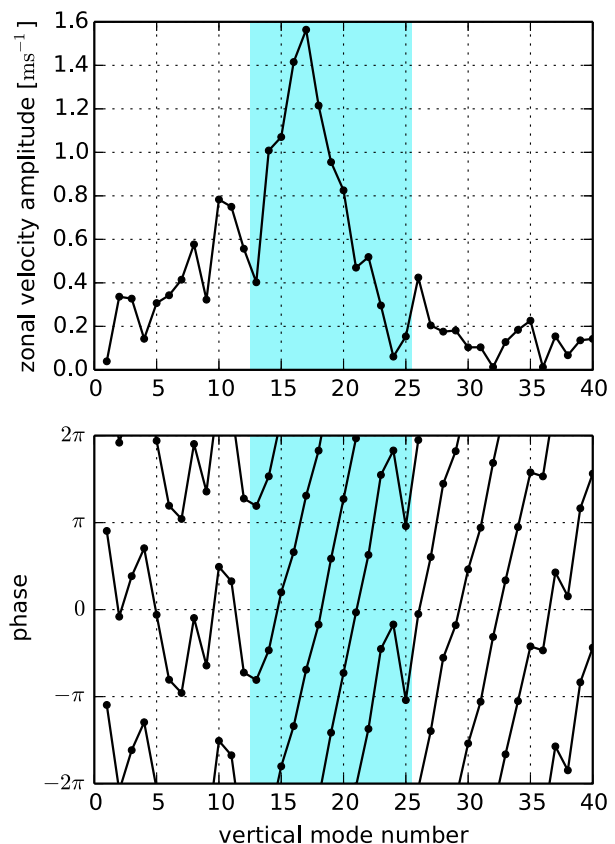

FIG. 4. (top) Amplitude of zonal velocity projected onto the vertical normal modes, given by $2|a_{n\omega}|$, for the 1650-day period and (bottom) corresponding phase. The light blue shading on both panels indicates the range of modes used for filtering.
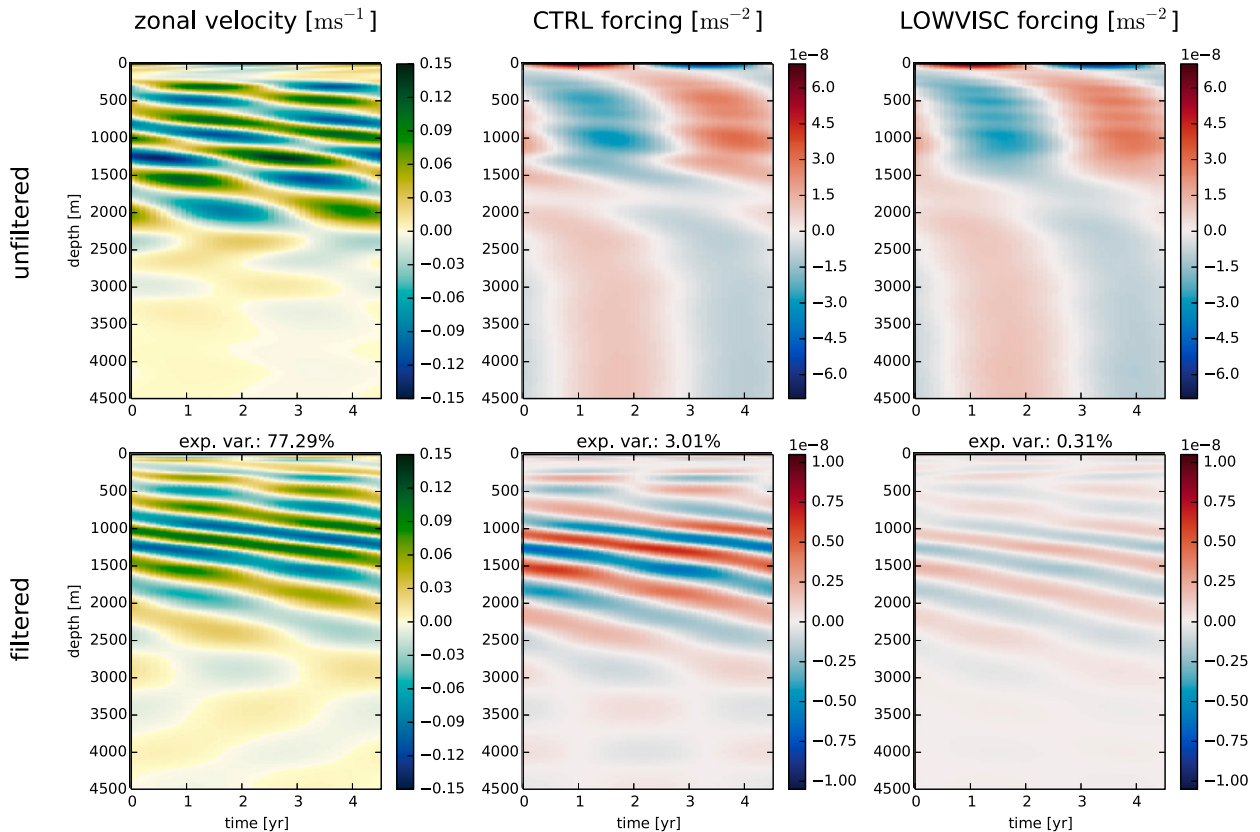
FIG. 5. (top) Unfiltered and (bottom) band-filtered signal of (left) zonal velocity at 23°W, diagnosed forcing based on (center) multi-mode configuration CTRL, and (right) LOWVISC. The filtered signals consist only of baroclinic modes 13 to 23 of the corresponding unfiltered one. Note the different color scale for the unfiltered and filtered forcing. The numbers given above the lower panels are the percentages of variance the filtered signal explains of the respective unfiltered signal.

gravity wave speed corresponds to the wave speed obtained from the mean stratification of the equatorial Atlantic (see section 2a). The dissipation is parameterized by lateral mixing of momentum (see Greatbatch et al. 2012). The lateral eddy viscosity is set to $300 \, \mathrm{m^2 \, s^{-1}}$, a value that creates a meridional broadening in the model that is comparable to that observed for Atlantic EDJs (Greatbatch et al. 2012; Claus et al. 2014) and that is consistent with an estimate by Brandt et al. (2008) based on an oxygen budget analysis. Periodic forcing, given by (4), is applied to the zonal momentum equation with the same period as the EDJs', specified here as 1650 days. The forcing is chosen to be spatially uniform since the zonal wavelength of the EDJs is comparable to the basin width and to avoid spurious interior Ekman pumping due to curl in the spatial structure of the forcing. Since the model results, and thereby the estimated forcing, might depend on the choice of lateral viscosity and possibly on the geometry of the model domain, two sensitivity experiments were conducted based on the configuration described above, which will

be denoted as CTRL. The first has a rectangular-shaped basin geometry and is referred to as BOX, and the second, which is referred to as LOWVISC, has a reduced lateral eddy viscosity of $50 \, \mathrm{m^2 \, s^{-1}}$, a value that is just large enough to avoid Rossby wave focusing due to beta dispersion in the center of the basin (Claus et al. 2014).

b. Method

Since the underlying dynamics are assumed to be linear (Johnson and Zhang 2003) and the observed EDJs are dominated by a single frequency, the frequency of the forcing for each mode is set equal to the frequency of the EDJs, corresponding to the period of 1650 days. The multimode model is driven to a steady-oscillating state for each mode with a forcing $\tilde{X}$ in the zonal momentum equation, given by

$$\tilde{X}(t) = e^{i\omega_0 t} + e^{-i\omega_0 t}, \qquad (4)$$

where ω_0 is the angular frequency associated with the observed EDJs as diagnosed in section 2c.

In the steady-oscillating state, the model-computed zonal velocity $\tilde{u}_n$ for vertical normal mode n is fully described by a spatially dependent, complex-valued coefficient b_n, such that

$$\tilde{u}_n(\lambda, \theta, t) = b_n(\lambda, \theta)e^{i\omega_0 t} + b_n^*(\lambda, \theta)e^{-i\omega_0 t}, \quad (5)$$

where λ is longitude and θ is latitude. Since the amplitude of the forcing $\tilde{X}$ is identical for all modes, $|b_n|$ contains information about the resonance characteristics of each mode at the given frequency ω_0, with $|b_n|$ being relatively large when a resonant basin mode is excited. Using $b_n = |b_n|e^{i\phi_n}$, ϕ_n conveys the phase of $\tilde{u}_n$ relative to the forcing. In this notation, the more positive the phase, the earlier the occurrence in time.

The next step is to adjust the multimode model solution so that it corresponds to the fitted observed zonal velocity on the equator at 23°W, given by $a_{n\omega_0}$ in (2). Therefore, for each mode, the simulated zonal velocity fluctuation, represented by b_n, is scaled and phase shifted by multiplication with a complex coefficient f_n, which is simply given by

$$f_n = \frac{a_{n\omega_0}}{b_n(\lambda_0, \theta_0)}, \quad (6)$$

where (λ_0, θ_0) are the coordinates of the grid point closest to the location of the mooring where the observations were taken. Because of the linearity of the multimode model, this corresponds to a scaling and phase shifting of the forcing of the multimode model. Hence, the set f_n describes the time–depth structure of the forcing X, which is required to drive the observed EDJ signal in a linear system and is given by

$$X(z, t) = \sum_{n=1}^{N} (f_n e^{i\omega_0 t} + f_n^* e^{-i\omega_0 t})\hat{p}_n(z). \quad (7)$$

The basinwide signal of the fitted EDJs, as they are represented in the multimode model, can be reconstructed by scaling the multimode model solution with the set f_n, so that

$$u(\lambda, \theta, z, t) = \sum_{n=1}^{N} [f_n b_n(\lambda, \theta)e^{i\omega_0 t} + f_n^* b_n^*(\lambda, \theta)e^{-i\omega_0 t}]\hat{p}_n(z). \quad (8)$$

An inevitable consequence of the formulation of (6) is the sensitivity of the forcing to nonresonant modes. At the equator, b_n is relatively small for these modes, which leads for a nonzero $a_{n\omega_0}$ to a large f_n compared to that for resonant modes. This might contaminate the estimate of the forcing. To overcome this issue, a filter may be applied by considering only a subset Γ of

vertical modes in the estimation of the forcing [(7)] and the reconstruction of the basinwide zonal velocity signal [(8)]. Here, the choice of Γ is based on the amplitudes of the coefficients $a_{n\omega_0}$ and their phase relation. To isolate the modes that dominantly contribute to the signal with downward phase propagation, shown in Fig. 4, the baroclinic spectrum was subsampled to a contiguous band of modes that contains the dominant mode 17 and for which the phase increases with increasing mode number. The band Γ chosen here spans modes 13 to 23 (indicated by the blue shading in Fig. 4).

c. Results

As mentioned in the previous subsection, it is necessary to filter out modes of minor importance and the filter is chosen to span modes 13 to 23. As shown in Fig. 5, the filtered velocity signal, obtained from (8) using a range of n from 13 to 23, is similar to the unfiltered one using a range of n from 1 to 40, especially above 2500-m depth. This can be quantified by noting that the filter retains 78% of the variance of the unfiltered signal. Although the filtering largely preserves the velocity, it drastically alters the estimate of the required forcing. As can be seen from Fig. 5, the filtered forcing obviously lacks the large vertical scale structure present in the unfiltered version since the low baroclinic modes, which are far from resonance at the forcing period, have been eliminated. The results show that the variance of the filtered forcing explains about 3% of the variance of the unfiltered forcing; however, the signal produced by the filtered forcing still explains 78% of the variance of the unfiltered signal in the zonal velocity. Hence, only a small fraction of the forcing is needed to produce most of the velocity signal, which clearly emphasizes the importance of resonance for the dynamics of the EDJs. The filtered forcing signal has a notably similar vertical time structure as the EDJs; in particular, it solely exhibits downward phase propagation in the depth range between 500 and 3000 m, which is consistent with the idea of in situ maintenance of the EDJs by the forcing (Ascani et al. 2015).

Since the vertical structure of the forcing is now determined, the basinwide signature of the EDJs can be reconstructed by evaluating the filtered version of (8). In what follows, this reconstruction will be validated against independent observations. Figure 6 shows reconstructed zonal velocity along the equator on 1 June 2001, together with the amplitude and phase of zonal velocity along the equator and estimates of both zonal and vertical wavelengths. Here, the local wavelengths are determined by the inverse of the
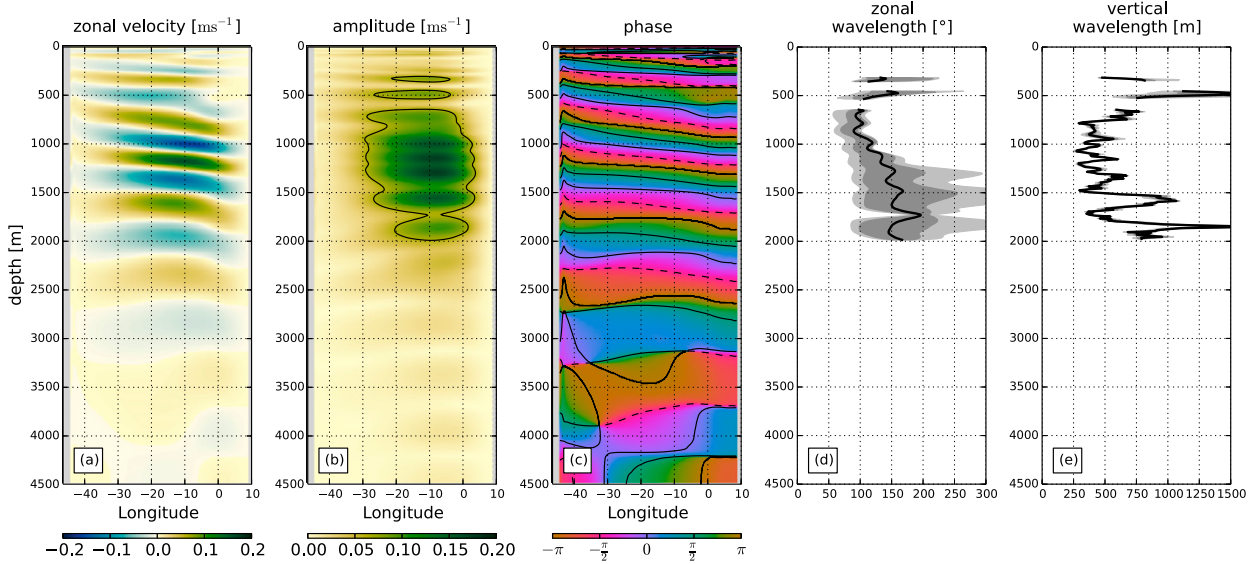
FIG. 6. Reconstruction of the 1650-day zonal velocity variability along the equator using the multimode experiment CTRL. (a) Snapshot of zonal velocity corresponding to 1 Jun 2001. (b) Amplitude of the zonal velocity oscillation. The contour line corresponds to e^{-1} of the overall maximum. (c) Associated phase. (d) Distribution of local zonal wavelength in degrees longitude, estimated where the amplitude exceeds e^{-1} of its maximum. Shown is the median as a solid line and values between the 25th and 75th percentile are shaded in dark gray and between the 5th and 95th percentile in lighter gray. (e) As in (d), but for the vertical wavenumber.

zonal and vertical derivative of phase, respectively, that is

$$\lambda_x = 2\pi \left| \frac{\partial x}{\partial \phi} \right| \quad \text{and} \quad \lambda_z = 2\pi \left| \frac{\partial z}{\partial \phi} \right|, \qquad (9)$$

where ϕ is the phase and these wavelengths are only determined where the amplitude exceeds e^{-1} of the overall maximum amplitude. The instantaneous zonal velocity clearly shows a downward slope of the reconstructed EDJs toward the east above 2000 m, and the associated phase indicates a westward and downward phase propagation, a feature that is also observed for the Atlantic EDJs (Johnson and Zhang 2003; Youngs and Johnson 2015). The amplitude has little zonal structure with distinct, vertically staggered maxima at 10°W, which are separated in the vertical by about 300 m. The overall maximum amplitude of zonal velocity is found at 1300-m depth, which is again in agreement with direct observations of zonal velocity (Gouriou et al. 2001; Bourlès et al. 2003) and density (Youngs and Johnson 2015). The zonal positions of these maxima are controlled by the lateral mixing applied in the model configuration. In the (near) inviscid limit, the maximum amplitude of an equatorial basin mode is located in the center of the basin; increasing the eddy viscosity leads to an eastward shift of this maximum (Claus et al. 2014). The estimated range of vertical wavelengths of 300 to 700 m agrees very well

with observations (Gouriou et al. 2001; Bourlès et al. 2003; Johnson and Zhang 2003; Bunge et al. 2008; Youngs and Johnson 2015) and the zonal wavelength at the equator is about 80° to 200° in the multimode representation, which is shorter than the zonal wavelength of an equatorial Kelvin wave (215°) being associated with the dominant vertical mode and frequency of the EDJs and longer than the respective gravest equatorial Rossby wave (72°; see also Fig. 7). On the equator, the Rossby wave and Kelvin wave components of the resonant equatorial basin mode of the dominant vertical mode superimpose, which may lead to the broad range of zonal wavenumber estimates on the equator. For the dominant vertical wavelength, Youngs and Johnson (2015) estimated the zonal wavelength of the EDJs' Rossby wave component by a plane wave fit to vertical strain profiles at about 1.5° N/S, where they found maximum variance in vertical strain. For a linear equatorial Rossby wave, these vertical strain maxima are associated with minima of zonal velocity amplitude, which are close to 1.5° N/S in the reconstructed zonal velocity, as shown in Fig. 7. At about 2.5° N/S, where the amplitude of the reconstructed zonal velocity has off-equatorial maxima, the estimated zonal wavelength matches the theoretically predicted 72° (Fig. 7) and is consistent with the estimate by Youngs and Johnson (2015). Overall, the reconstructed zonal velocity signal and independent observations of the EDJs in the Atlantic (observations not used as input for
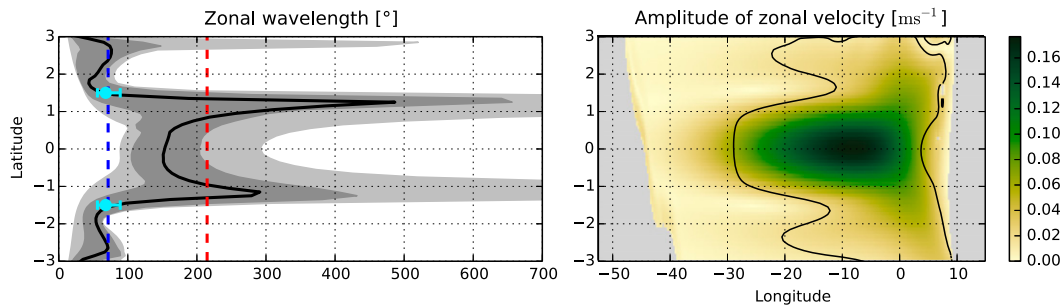
FIG. 7. (left) Zonal wavelength estimated from the reconstructed zonal velocity variability at 1300-m depth. Shown is the median as a solid line and values between the 25th and 75th percentile are shaded in dark gray and between the 5th and 95th percentile in lighter gray. The blue dashed line indicates the zonal wavelength of the gravest inviscid long equatorial Rossby wave associated with the dominant vertical mode and frequency of the EDJs, and the red dashed line is the wavelength of the respective equatorial Kelvin wave. Estimates by Youngs and Johnson (2015) are shown as blue circles and error bars. (right) Amplitude of zonal velocity fluctuations associated with the EDJs at 1300-m depth. The black line encloses the region in which the zonal wavelength is estimated.

the reconstruction) are in good agreement on the equator and in its proximity.

With the reconstructed zonal velocity and the estimated forcing, the resulting power input can be computed. The zonally averaged, time-mean power input on the equator, shown in Fig. 8, peaks at the same depth as the maximum zonal velocity amplitude (cf. Fig. 6). Above 2500 m, the forcing actively maintains the EDJ signal, whereby most of the power input is located between 1000 and 1750 m. There, the maxima in power input are at similar depths as the maxima in velocity amplitude, suggesting that the forcing and the EDJ signal are in phase in this depth range. The scaled multimode model response also provides a reconstruction of perturbation pressure p' and vertical velocity w. Hence, it is possible to diagnose the zonally averaged, time-mean, vertical energy flux $\overline{wp'}$, which is also shown in Fig. 8. Upward propagation of energy is prevailing throughout the water column and its vertical profile is in close correspondence to the power input. Hence, the divergence of vertical energy flux cannot solely balance the power input, indicating the importance of other terms in the energy balance such as the divergence of the horizontal energy flux and dissipation. Indeed, in the horizontally integrated energy budget, the only term that can balance the power input at 1300-m depth is the dissipation.

In the presence of strong dissipation, as assumed here, the apparent vertical propagation is closely linked to the vertical time structure of the forcing shown in Fig. 5. The individual jets have difficulty to propagate more than a vertical wavelength and hence the forcing must project instantaneously onto the EDJs in order to maintain them. Consequently, the forcing exhibits a

similar vertical propagation as the EDJs. Furthermore, the strong dissipation and the lack of forcing below 2500-m depth justify the assumption of a flat bottom implicit in the use of vertical normal modes.

To identify the influence of the basin geometry and the amount of damping on the model solutions, two additional multimode runs, BOX and LOWVISC, were conducted (see section 3a). As it turned out, the
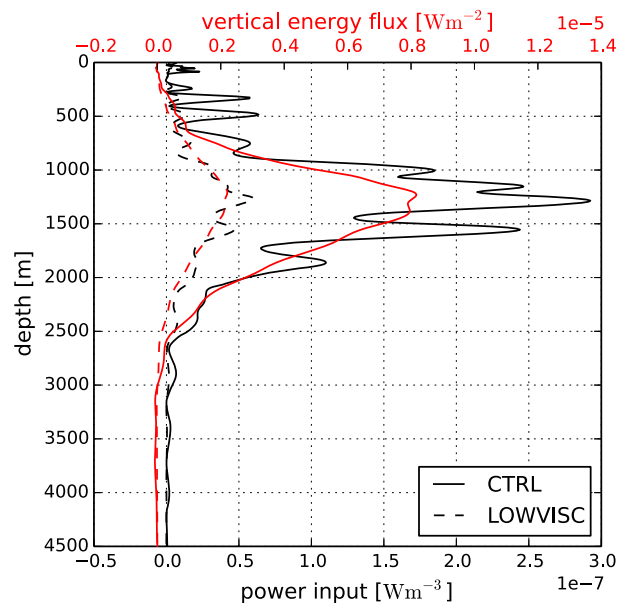

FIG. 8. (black) Power input and (red) the vertical flux of energy for the 1650-day variability based on the experiments CTRL (solid lines) and LOWVISC (dashed lines). Both the power input and the vertical energy flux are averaged over one period and along the equator. A reference density of $1024\ kg\ m^{-3}$ was used for unit conversion.
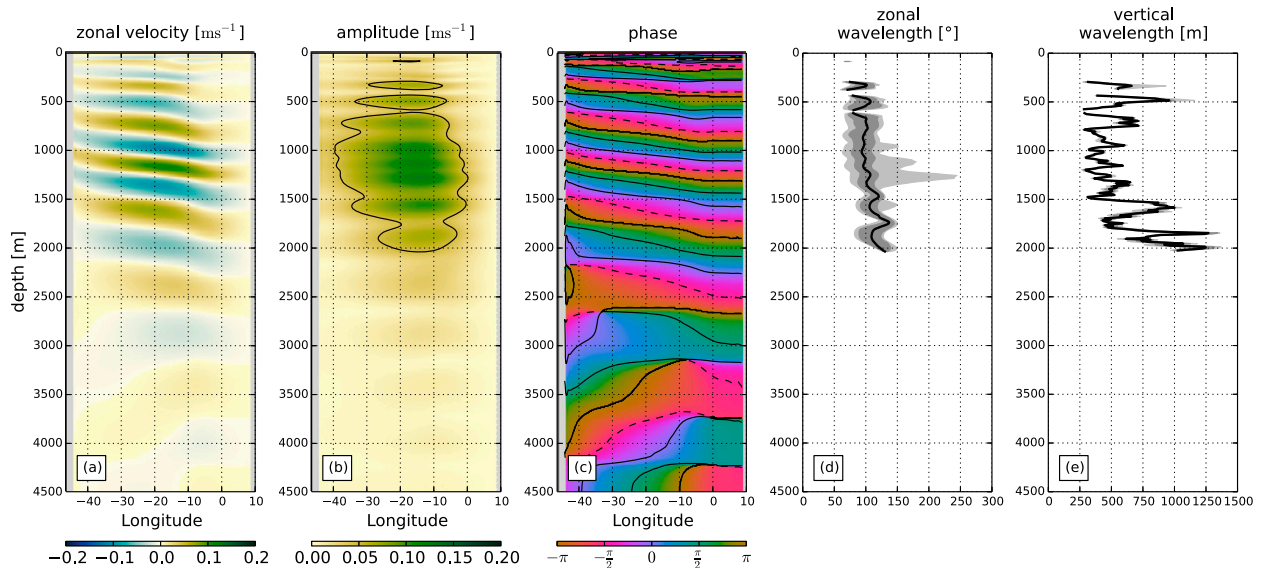
FIG. 9. As in Fig. 6, but based on multimode experiment LOWVISC.

results of BOX are almost indistinguishable from the previous results (not shown), which indicates that the details of the basin geometry do not have a significant impact on the amplitude and phase of zonal velocity along the equator associated with vertical modes 13 to 23. Figure 9 shows the reconstructed zonal velocity signal along the equator using the LOWVISC output. The amplitude maxima are at the same depth level as for CTRL but, as expected, shifted to the west. Compared to CTRL, the regions where the amplitude exceeds e^{-1} of its maximum do cover a broader zonal range, and the estimated zonal wavelength is more uniform with depth. The vertical wavenumber, however, is not affected by the choice of eddy viscosity, and the meridional width is 20% smaller than observed and 25% smaller than for CTRL. Generally, the maximum amplitude of zonal velocity is 25% lower compared to CTRL, since, because of the westward shift of the zonal velocity maximum with decreasing eddy viscosity, less forcing is required to produce the same signal at 23°W where the multimode model is fitted. This is also evident from the forcing derived on the basis of LOWVISC output, shown in Fig. 5. While the unfiltered forcing compares well with CTRL, the filtered forcing is considerably weaker. However, the structure of the vertical profiles of the power input and vertical energy flux agree well for both cases, as shown in Fig. 8, which shows that the relationship between the power input and the vertical energy flux is not dependent on the choice of lateral eddy viscosity but is an intrinsic feature of the dynamics. These qualitative and quantitative agreements of CTRL, BOX, and LOWVISC argue for the robustness of the results presented here.

4. Summary and discussion

We have used a linear multimode shallow-water model, consisting of one independent shallow-water model for each vertical normal mode, to estimate the vertical structure of the forcing that is required to drive a linear representation of the equatorial deep jets (EDJs) as they are observed at 23°W on the equator. The model was set up to resemble the equatorial Atlantic basin, and the forcing frequency was determined from moored observations at 23°W. We showed that more than 50% of the observed zonal flow variability at the mooring location may be represented by oscillations at three distinct periods: the semiannual cycle, the annual cycle, and the EDJs' period of 1650 days. Each of these three periods have the most energy in the vertical normal modes that form resonant baroclinic equatorial basin modes at these periods, indicating the crucial importance of linear equatorial dynamics for the given modes of variability. The zonal velocity variability could be explained not only at intermediate depth, but also in the depth range occupied by the Equatorial Undercurrent (EUC), whose variability at annual and semiannual time scales can be linked to basin-mode resonance (Brandt et al. 2016). For the EDJs, the importance of resonance was demonstrated by subsampling the baroclinic modes, by which we could show that 3% of the diagnosed forcing variance drives 78% of the velocity variance. The subsampled

forcing closely resembles the vertical structure of the EDJs over a considerable depth range and hence supports the hypothesis of in situ maintenance of the jets (Ascani et al. 2015) between 500 and 2500 m.

We were also able to faithfully reconstruct the EDJ signal along the equator, where especially the zonal wavelength of the jets, the zonal distribution of amplitude, and the meridional width are sensitive to the choice of lateral eddy viscosity. Confirmation of these three quantities through additional, deep-reaching, moored zonal velocity observations along and across the equator (within 1° either side) would help to further assess the intensity of lateral mixing in the multimode model and to reduce the uncertainty in the estimated forcing. The zonal velocity has a vanishing amplitude below 2500-m depth, regardless of the model configuration used for the reconstruction, which is well above the crest of the Mid-Atlantic Ridge. Hence, the EDJs are unlikely to feel the influence of the bottom topography, making the assumption of a flat bottom appropriate.

One puzzling aspect of EDJ observations is the absence of upward phase and downward energy propagation. Since the source of energy is at intermediate depth, the energy should propagate away in both directions, up and down. However, the diagnosed forcing solely exhibits downward phase propagation and projects only onto jets having downward phase and upward energy propagation. Hence, any signal having upward phase and downward energy propagation is not reinforced and decays relatively quickly, compared to the period of the EDJs, due to strong dissipation. Consequently, the prevailing downward phase propagation of the EDJs requires the forcing to also have downward phase propagation, a finding that is robust with respect to the choice of lateral eddy viscosity or basin geometry. In the context of nonlinear interaction of two intraseasonal Yanai waves, as proposed by Ascani et al. (2015) as a possible driving mechanism for the EDJs, the requirement for their product to have a downward phase propagation only allows for certain combinations of waves. Long-lasting observations of zonal and meridional velocity in the intermediate depth range of the Atlantic Ocean might help to identify possible pairs of waves, whose nonlinear product projects onto the diagnosed forcing structure and hence are able to drive the EDJs.

One major simplification in the model setup was the assumption of a uniform horizontal structure of the forcing. This choice was motivated by the fact that the zonal wavelength of the EDJs is up to twice as long as the equatorial Atlantic basin, which implies that the jets themselves have little zonal structure apart from the

requirement to fit the basin width. Additionally, a uniform forcing mitigates spurious Ekman pumping off the equator and, consequently, only excites equatorial waves and coastal Kelvin waves. We acknowledge that the uniform zonal structure of the forcing likely has an impact on the estimated power input; however, there is no good reason to choose any other structure without further knowledge of the governing driving mechanism. Additionally, a lack of power input by the forcing off the equator in all model configurations (not shown) supports the suitability of a uniform meridional forcing structure.

Given the similarity in basin width and EDJ scales of the Atlantic and Indian Oceans (Youngs and Johnson 2015), we suggest that the results presented here can be transferred to the Indian Ocean; however, noting that for final certainty, observations of sufficient quality in the Indian Ocean are missing at present. In the Pacific, the basin is approximately 3 times wider compared to the Atlantic. Additionally, the EDJs are of smaller vertical scale and hence are associated with higher vertical modes, resulting in periods about 3 times longer than in the Atlantic (Youngs and Johnson 2015). Based on the scaling argument of Greatbatch et al. (2012) and the scales provided by Youngs and Johnson (2015), the eddy viscosity that is needed to broaden the EDJs by 50% in the Pacific is about one-third of that required in the Atlantic. It remains unclear at this point why the effective viscosity in the Pacific must be lower than in the Atlantic Ocean. One possible process leading to dissipation of the EDJs and being mimicked by the lateral mixing of momentum is the cross-equatorial advection of the EDJs by intraseasonal Yanai waves as suggested by synoptic observations (Muench et al. 1994; Gouriou et al. 2001; Dengler and Quadfasel 2002; Bourlès et al. 2003). The advection of the jet cores disrupts their geostrophic balance and hence results in the shedding of gravity waves and loss of EDJ energy. Another possibility, as pointed out by Ascani et al. (2015), is the nonlinear self-interaction of the EDJs via the uu_x term in the zonal momentum balance that acts as a sink of energy for the EDJs in the model used by Ascani et al. (2015; see also Greatbatch 1985, his section 6). Both processes may differ in strength in the Atlantic and Pacific Oceans, which might result in different eddy viscosities in these basins. However, a careful observational analysis of the cross-equatorial structure, a possible meridional migration of the EDJs, and the magnitude of the nonlinear self-advection would be required to shed light on this problem.

Finally, we want to emphasize that the method presented in this work, which is fitting of a multimode shallow-water model to observations, can be applied to

a range of linear problems covering externally driven or strongly periodic variability in regions where bathymetry is not important. Its power relies on the fact that the vertical structure of the forcing is not required a priori but is obtained by least squares fitting to observations. One possible application, to be discussed elsewhere, is the fitting of sea surface height from a wind-driven equatorial multimode model to altimeter data, which could improve our understanding of the time-varying equatorial circulation.

REFERENCES

Ascani, F., E. Firing, P. Dutrieux, J. P. McCreary, and A. Ishida, 2010: Deep equatorial ocean circulation induced by a forced–dissipated Yanai beam. *J. Phys. Oceanogr.*, **40**, 1118–1142, doi:10.1175/2010JPO4356.1.

——, ——, J. P. McCreary, P. Brandt, and R. J. Greatbatch, 2015: The deep equatorial ocean circulation in wind-forced numerical solutions. *J. Phys. Oceanogr.*, **45**, 1709–1734, doi:10.1175/JPO-D-14-0171.1.

Bourlès, B., and Coauthors, 2003: The deep currents in the eastern equatorial Atlantic Ocean. *Geophys. Res. Lett.*, **30**, 8002, doi:10.1029/2002GL015095.

Brandt, P., V. Hormann, B. Bourlès, J. Fischer, F. A. Schott, L. Stramma, and M. Dengler, 2008: Oxygen tongues and zonal currents in the equatorial Atlantic. *J. Geophys. Res.*, **113**, C04012, doi:10.1029/2007JC004435.

——, A. Funk, V. Hormann, M. Dengler, R. J. Greatbatch, and J. M. Toole, 2011: Interannual atmospheric variability forced by the deep equatorial Atlantic Ocean. *Nature*, **473**, 497–500, doi:10.1038/nature10013.

——, and Coauthors, 2012: Ventilation of the equatorial Atlantic by the equatorial deep jets. *J. Geophys. Res.*, **117**, C12015, doi:10.1029/2012JC008118.

——, M. Claus, R. J. Greatbatch, R. Kopte, J. M. Toole, W. E. Johns, and C. W. Böning, 2016: Annual and semi-annual cycle of equatorial Atlantic circulation associated with basin-mode resonance. *J. Phys. Oceanogr.*, doi:10.1175/JPO-D-15-0248.1, in press.

Bunge, L., C. Provost, B. L. Hua, and A. Kartavtseff, 2008: Variability at intermediate depths at the equator in the Atlantic Ocean in 2000–06: Annual cycle, equatorial deep jets, and intraseasonal meridional velocity fluctuations. *J. Phys. Oceanogr.*, **38**, 1794–1806, doi:10.1175/2008JPO3781.1.

Cane, M. A., and D. W. Moore, 1981: A note on low-frequency equatorial basin modes. *J. Phys. Oceanogr.*, **11**, 1578–1584, doi:10.1175/1520-0485(1981)011<1578:ANOLFE>2.0.CO;2.

Claus, M., R. J. Greatbatch, and P. Brandt, 2014: Influence of the barotropic mean flow on the width and the structure of the Atlantic equatorial deep jets. *J. Phys. Oceanogr.*, **44**, 2485–2497, doi:10.1175/JPO-D-14-0056.1.

Dengler, M., and D. Quadfasel, 2002: Equatorial deep jets and abyssal mixing in the Indian Ocean. *J. Phys. Oceanogr.*, **32**, 1165–1180, doi:10.1175/1520-0485(2002)032<1165:EDJAAM>2.0.CO;2.

Dietze, H., and U. Loeptien, 2013: Revisiting "nutrient trapping" in global coupled biogeochemical ocean circulation models. *Global Biogeochem. Cycles*, **27**, 265–284, doi:10.1002/gbc.20029.

D'Orgeville, M., B. L. Hua, and H. Sasaki, 2007: Equatorial deep jets triggered by a large vertical scale variability within the western boundary layer. *J. Mar. Res.*, **65**, 1–25, doi:10.1357/002224007780388720.

Eden, C., and M. Dengler, 2008: Stacked jets in the deep equatorial Atlantic Ocean. *J. Geophys. Res.*, **113**, 1–12, doi:10.1029/2007JC004298.

Eriksen, C. C., 1982: Geostrophic equatorial deep jets. *J. Mar. Res.*, **40**, 143–157.

Firing, E., 1987: Deep zonal currents in the central equatorial Pacific. *J. Mar. Res.*, **45**, 791–812, doi:10.1357/002224087788327163.

——, S. E. Wijffels, and P. Hacker, 1998: Equatorial subthermocline currents across the Pacific. *J. Geophys. Res.*, **103**, 21 413–21 423, doi:10.1029/98JC01944.

Getzlaff, J., and H. Dietze, 2013: Effects of increased isopycnal diffusivity mimicking the unresolved equatorial intermediate current system in an Earth system climate model. *Geophys. Res. Lett.*, **40**, 2166–2170, doi:10.1002/grl.50419.

Gill, A. E., 1982: *Atmosphere–Ocean Dynamics.* Academic Press, 662 pp.

Gouriou, Y., and Coauthors, 2001: Deep circulation in the equatorial Atlantic Ocean. *Geophys. Res. Lett.*, **28**, 819–822, doi:10.1029/2000GL012326.

Greatbatch, R. J., 1985: Kelvin wave fronts, Rossby solitary waves and the nonlinear spin-up of the equatorial oceans. *J. Geophys. Res.*, **90**, 9097–9107, doi:10.1029/JC090iC05p09097.

——, P. Brandt, M. Claus, S.-H. Didwischus, and Y. Fu, 2012: On the width of the equatorial deep jets. *J. Phys. Oceanogr.*, **42**, 1729–1740, doi:10.1175/JPO-D-11-0238.1.

Hayes, S. P., and H. B. Milburn, 1980: On the vertical structure of velocity in the eastern equatorial Pacific. *J. Phys. Oceanogr.*, **10**, 633–635, doi:10.1175/1520-0485(1980)010<0633:OTVSOV>2.0.CO;2.

Hua, B. L., M. D'Orgeville, M. D. Fruman, C. Ménesguen, R. Schopp, P. Klein, and H. Sasaki, 2008: Destabilization of mixed Rossby gravity waves and the formation of equatorial zonal jets. *J. Fluid Mech.*, **610**, 311–341, doi:10.1017/S0022112008002656.

Johns, W. E., P. Brandt, B. Bourlès, A. Tantet, A. Papapostolou, and A. Houk, 2014: Zonal structure and seasonal variability of the Atlantic Equatorial Undercurrent. *Climate Dyn.*, **43**, 3047–3069, doi:10.1007/s00382-014-2136-2.

Johnson, G. C., and D. Zhang, 2003: Structure of the Atlantic Ocean equatorial deep jets. *J. Phys. Oceanogr.*, **33**, 600–609, doi:10.1175/1520-0485(2003)033<0600:SOTAOE>2.0.CO;2.

——, E. Kunze, K. E. McTaggart, and D. W. Moore, 2002: Temporal and spatial structure of the equatorial deep jets in the Pacific Ocean. *J. Phys. Oceanogr.*, **32**, 3396–3407, doi:10.1175/1520-0485(2002)032<3396:TASSOT>2.0.CO;2.

Leetmaa, A., and P. F. Spain, 1981: Results from a velocity transect along the equator from 125 to 159°W. *J. Phys. Oceanogr.*, **11**, 1030–1033, doi:10.1175/1520-0485(1981)011<1030:RFAVTA>2.0.CO;2.

Luyten, J. R., and J. Swallow, 1976: Equatorial undercurrents. *Deep-Sea Res. Oceanogr. Abstr.*, **23**, 999–1001, doi:10.1016/0011-7471(76)90830-5.

Matthießen, J.-D., R. J. Greatbatch, P. Brandt, M. Claus, and S.-H. Didwischus, 2015: Influence of the equatorial deep jets on the North Equatorial Countercurrent. *Ocean Dyn.*, **65**, 1095–1102, doi:10.1007/s10236-015-0855-5.

Ménesguen, C., B. L. Hua, M. D. Fruman, and R. Schopp, 2009: Dynamics of the combined extra-equatorial and equatorial deep jets in the Atlantic. *J. Mar. Res.*, **67**, 323–346, doi:10.1357/002224009789954766.

Muench, J. E., and E. Kunze, 1999: Internal wave interactions with equatorial deep jets. Part I: Momentum-flux divergences. *J. Phys. Oceanogr.*, **29**, 1453–1467, doi:10.1175/1520-0485(1999)029<1453:IWIWED>2.0.CO;2.

——, and ——, 2000: Internal wave interactions with equatorial deep jets. Part II: Acceleration of the jets. *J. Phys. Oceanogr.*, **30**, 2099–2110, doi:10.1175/1520-0485(2000)030<2099:IWIWED>2.0.CO;2.

——, ——, and E. Firing, 1994: The potential vorticity structure of equatorial deep jets. *J. Phys. Oceanogr.*, **24**, 418–428, doi:10.1175/1520-0485(1994)024<0418:TPVSOE>2.0.CO;2.

Youngs, M. K., and G. C. Johnson, 2015: Basin-wavelength equatorial deep jet signals across three oceans. *J. Phys. Oceanogr.*, **45**, 2134–2148, doi:10.1175/JPO-D-14-0181.1.